Egy. J. Pure & Appl. Sci. 2024; 62(3):1-18

Egyptian Journal of Pure and Applied Science

Highly accurate phase unwrapping algorithm applied to comparative measurement in phase-shifting digital interferometry

Nasser A. Moustafa [1*], A. E. Elmahdy [1]

[1] *Helwan University, Faculty of Science, Physics Department, Cairo, Egypt*

ARTICLE INFO

Received 18 March 2024
Accepted 17 April 2024

Keywords
Speckle interferometry,
Difference correlation fringes,
Comparative measurement,
Phase unwrapping algorithm,
Photo-refractive materials,
Sum correlation fringes.

Correspondence
Nasser A. Moustafa
E-mail*
(Corresponding Author)
nassermoustafa@gmail.com

ABSTRACT

This study introduces comparative speckle pattern interferometry as a method to visually compare two comparable items, namely the master and the test. The comparison result is displayed as an interference pattern that illustrates the displacement difference. Using the stored master and test objects in the photorefractive material ($LiNbO_3$ crystal), different phase-stepping algorithms are implemented. A new formula for the addition of the difference and sum phases of deformations and the error in the calculated phase is obtained using three-, four-, and five-phase step algorithms. The difference correlation fringes that coexist with the sum correlation fringes can be obtained and analyzed using the unwrapped phase maps extract only the difference fringe map that corresponds to the difference correlation fringes and measure the difference in displacement accurately and with high performance. The results show that the five-phase stepping method gives more accurate results than the three- and four-phase stepping methods when looking at the unwrapped phase map of the difference in displacement between the two stressed objects..

1. Introduction

Traditional holographic and speckle interferometry cannot directly compare two identical specimens under similar stress conditions. Each displacement field must be calculated independently to ascertain the difference in displacement between the two object surfaces. Only then can the numerical results be compared. However, in fact, even for small strains, holographic and speckle interferometry cause fringe overcrowding.

Without strong magnification, the fringe system becomes too dense to observe, making the evaluation laborious and occasionally even impossible. To mitigate or go around these challenges, a few comparative holographic and interferometric approaches [1–4] have been developed. Comparative holographic and comparative speckle pattern interferometry, which show the variations in surface displacements of two similar specimens under the same stress level, have created a wealth of new possibilities for nondestructive testing and control.

To assure the highest level of measurement accuracy, phase-shifting and phase-unwrapping algorithms [5–12] are utilized. A highly accurate phase unwrapping algorithm applied to comparative measurement in phase-shifting digital interferometry is introduced. The synthetic lithium niobate ($LiNbO_3$) crystals were first produced in 1949 by Matthias and Remeika [13]. The crystals are classified under the rhombohedral (trigonal) space group $R3C$ and have a $3m$point group (C6v in Schonflies notation) [14]. Furthermore, it has an ABO3-type ferroelectric nature, characterized by an oxygen octahedron structure.

The novel approach relies on substituting the traditional method with the $LiNbO_3$ crystal as the recording medium [1, 2]. To extract only the difference fringe map that corresponds to the difference correlation fringes and measure the difference in displacement accurately and with high performance, the difference correlation fringes that coexist with the sum correlation fringes can be obtained and analyzed using the unwrapped phase maps. The provided results demonstrate that the five-phase stepping algorithm yields more accurate results than the three- and four-phase stepping algorithms when it comes to the unwrapped phase map of the difference in displacement of the two stressed objects.

2. Optical setup

The master (MO) and test (TO) items, motorized linear translation stages, reference wave (bump beam) with average intensity I_2, and $LiNbO_3$ with a 5 mm x 5 mm x 5 mm size are the fundamental components of the experimental setup (Fig. 1). One coherent low-power laser beam (λ=670 nm and P=10 mW) is the light source. CCD camera with 4.65 × 4.65 pixel size and 1280 x 1024 pixel resolution. For automatic fringe analysis, the phase shifts needed are obtained using a piezoelectric transducer (PZT). There were two identical bars that needed to be compared. It is possible to move the bars vertically, axially, or by rotating them about their vertical axis.

3. The analysis of the interference pattern

During the comparison procedure, the hologram of the master object replaces it in this comparable digital approach. One benefit of this replacement is that it always compares results using the same non-displaced and displaced patterns. Fig 1 shows the arrangement. To supply the micro displacement, the master and test objects are placed on a linear motorized translation stage.

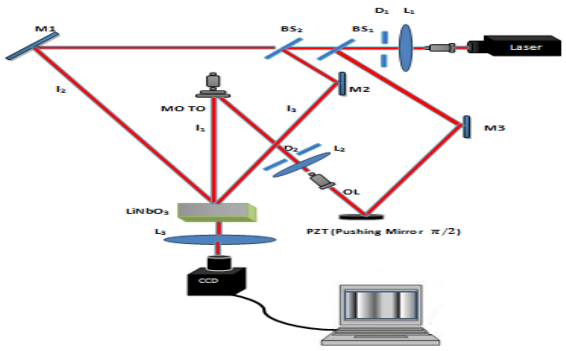

Fig. 1 Experimental set-up for comparative measurement in speckle interferometry using a single reference beam technique with $LiNbO_3$ Crystal as a recording medium: OL: objective lens, L_1, and L_2: lenses, D1 and D2: pupil apertures, BS: beam splitter, L_3: imaging lens, Crystal $LiNbO_3$ (CCD): observation plane, M_1 and M_2: mirrors, I_1: average intensity of the object beam, I_2: average intensity of the pump beam. MO and TO: master and test objects.

Using a single reference beam, the experiment's first phase records and stores the speckle pattern of the master object's displaced and non-displaced states in the $LiNbO_3$ crystal [14, 15]. There are two parts in step two of the second stage: The first stage involves recording and storing in the computer's memory the non-displaced test item and the returned speckle pattern of the displaced and non-displaced states of the master object. The second step involves recording and restoring into the computer's memory the displaced state of the test object as well as the retrieved speckle pattern of the non-displaced and displaced states of the master object. The master and test objects are coupled to motorized linear translation stages based on their displacement states (axial or lateral states).

The following describes the basic processing of the operation: U_m and U_m' are the complex amplitudes of the master object that was retrieved, respectively, before and after displacement.

$$U_m = u_m e^{i\varphi_m} \quad (1)$$

$$U_m' = u_m' e^{i(\varphi_m + \varphi_m')} \quad (2)$$

Assume that U_t is the complex amplitude of the light scattered in the initial state by the test object.

$$U_t = u_t e^{i\varphi_t} \quad (3)$$

The wave field scattered by the test object in its displaced state is interfered with by the complex amplitude generated by the retrieved master object.

$$U_r = U_t + U_{mr} \quad (4)$$

where $U_{mr} = U_m + U_m'$ is the virtual images' complex amplitude that was extracted from the hologram.

The front panel of the CCD camera displays the following intensity distribution:

$$I = |U_t + U_{mr}|^2 = I_t + I_m + I_m' + 2\sqrt{I_m I_m'}\cos(\varphi_m') + 2\sqrt{I_t I_m}\cos(\Delta\varphi) + 2\sqrt{I_t I_m'}\cos(\Delta\varphi - \varphi_m') \quad (5)$$

where $\Delta\varphi = (\varphi_t - \varphi_m')$ is the phase difference that corresponds to the difference between the test and master objects' displaced and non-displaced states, where the master object is in its retrieved displaced state and the test object is in its non-displaced state. As previously indicated, the second step involves the CCD camera receiving the wave fields of the retrieved non-displaced and displaced states of the master object as well as the scattered light from the test object in its displaced state.

Let be the complex amplitude of the scattered light of the test object in its final (displaced) state, as in the preceding analysis:

$$U_t' = u_t' e^{i(\varphi_t + \varphi_t')} \quad (6)$$

where φ_t' is the phase term that was introduced because of the test object's displacement. The CCD camera's front panel's intensity is:

$$I' = |U_t' + U_{mr}|^2 = I_t' + I_m + I_m' + 2\sqrt{I_m I_m'}\cos(\varphi_m') + 2\sqrt{I_t' I_m}\cos(\Delta\varphi + \varphi_t') + 2\sqrt{I_t' I_m'}\cos(\Delta\varphi + \Delta\varphi') \quad (7)$$

where $\Delta\varphi' = (\varphi_t' - \phi_m')$ is the phase difference that corresponds to the difference between the test and master objects' displacement states, where the master object is in its retrieved displaced state and the test object is in its displaced state. The difference can be seen on the monitor by deducting the two images' resulting intensities I and I'. It is assumed that the two objects' displacements are sufficiently minimal such that $I_t \approx I_t'$ and $I_m \approx I_m'$.

$$\Delta I = I' - I = 2\sqrt{I_t I_m}[\cos(\Delta\varphi + \varphi_t') - \cos(\Delta\varphi - \varphi_m')] + 2\sqrt{I_t I_m}[\cos(\Delta\varphi + \Delta\varphi') - \cos(\Delta\varphi)] \quad (8)$$

i.e.

$$\Delta I = 4\sqrt{I_t I_m}\sin(\Delta\varphi + \tfrac{1}{2}\Delta\varphi')[\sin(\tfrac{1}{2}\Delta\varphi') + \sin(\tfrac{1}{2}\Delta\psi')] \quad (9)$$

where $\Delta\psi' = (\varphi_t' + \varphi_m')$ is the phase change caused by the sum of the two objects' displacements. Equation (9) illustrates that the first and second terms of the equation represent the difference in displacements between the two items and the sum of the displacements of the two objects, respectively. The two terms indicated in equation (9), which represent high-frequency random speckle noise, influence the sine component. The study culminates in the display of difference correlation fringes coexisting with sum correlation fringes as one fringe pattern.

3.1. Phase-stepping techniques and error due to a phase stepper error

As previously stated, the experimental setup utilized in the second part is identical to that of the first part, with the primary distinction being the only application of the phase-stepping technique in the second part through modifying one of the interferometer's mirrors on a PZT. To achieve the intended phase shifts between data frames, a precise calibration is required [6, 16]. For the three, four, and five phase step methods, a phase shift $\pi/2$ per exposure is used in present measurements. Three, four, and five phase-shifted intensity patterns can be created using the phase-shifting device. The intensity distribution of the correlograms can be written as:

$$\Delta I_N = 4\sqrt{I_t I_m}\sin(\Delta\varphi + \tfrac{1}{2}\Delta\varphi')[\sin(\tfrac{1}{2}\Delta\varphi' + \alpha_N) + \sin(\tfrac{1}{2}\Delta\psi' + \alpha_N)] \quad (10)$$

Where N = 1, 2,…., 5. Its value depends on the equation of the used phase stepping algorithm.

For three phase stepping algorithm, $\alpha_1 = \pi/4$, $\alpha_2 = 3\pi/4$, and $\alpha_3 = 5\pi/4$, for four phase stepping algorithm, $\alpha_1 = 0$, $\alpha_2 = \pi/2$, $\alpha_3 = \pi$, and $\alpha_4 = 3\pi/2$, and for five phase stepping algorithm, $\alpha_1 = 0$, $\alpha_2 = \pi/2$, $\alpha_3 = \pi$, and $\alpha_4 = 3\pi/2$, and $\alpha_5 = 2\pi$

Using the three, four, and five phase step algorithms from the intensity distributions of equation (10) one can derive a new formula for the sum of the difference and sum phases of deformations, which is as follows:

$$\Psi = (\Delta\varphi' + \Delta\psi') \quad (11)$$

For an algorithm using three phase stepping,

$$\Psi_3 = \arctan\left(\frac{\Delta I_3 - \Delta I_2}{\Delta I_1 - \Delta I_2}\right) \quad (12)$$

For an algorithm using four phase stepping,

$$\Psi_4 = \arctan\left(\frac{\Delta I_4 - \Delta I_2}{\Delta I_1 - \Delta I_3}\right) \quad (13)$$

For an algorithm using five phase stepping,

$$\Psi_5 = \arctan\left(\frac{2(\Delta I_2 - \Delta I_4)}{2\Delta I_3 - \Delta I_5 - \Delta I_1}\right) \quad (14)$$

For simplicity, fig. 2 shows the flowchart of processing 3,4, and 5 phase stepping algorithms .The majority of phase-shifting interferometric (PSI) approaches are mostly affected by the phase-stepper error [17, 18].

The phase step size is specified in phase shifting interferometry (PSI) methods and remains constant for the 3, 4, and 5 position approaches. The non-linearity in the motion of a PZT executing the phase-stepping or an incorrect phase-step size calibration could lead to an inaccurate estimation of the phase.

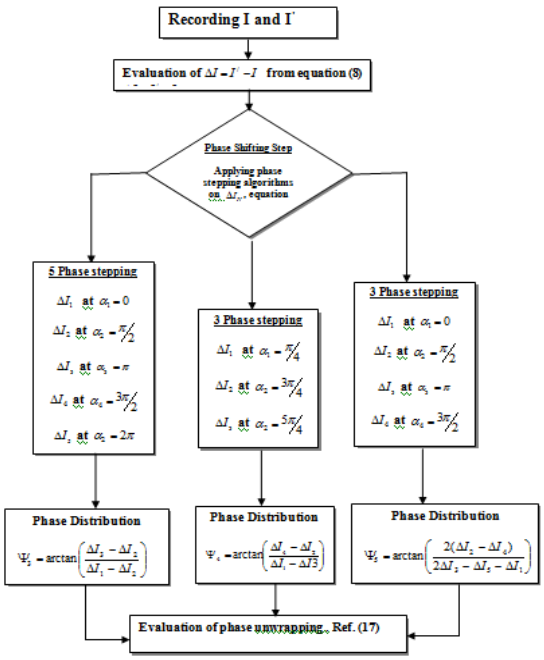

Fig. 2 Flowchart of processing 3, 4, and 5 phase stepping algorithms

The general equation for the phase map error $\Delta\Psi$ caused by the phase step error in the method that is being presented is as follows [19].

$$\Delta\Psi = \arctan\left[\frac{\sum_{r=1}^{R}\varepsilon_r - \sum_{r=1}^{R}\varepsilon_r \cos 2\alpha_r \cos 2\Psi - \sum_{r=1}^{R}\varepsilon_r \sin 2\alpha_r \sin 2\Psi}{R - \sum_{r=1}^{R}\varepsilon_r \cos 2\alpha_r \sin 2\Psi - \sum_{r=1}^{R}\varepsilon_r \sin 2\alpha_r \cos 2\Psi}\right] \quad (15)$$

Assuming that ε_r is small. Where $\Delta\Psi$ is the error in the calculated phase, Ψ is the calculated phase for the addition of the difference and sum phases of displacements, and α_r is the correct phase step.

The value of R can be changed from 3 to 5, depending on the phase step. In the present treatment, the value of R is chosen to be equal to 3, 4, and 5 respectively and $\varepsilon_r = \pi/20$. From equations (11-14) and (15), and after the simplification, the new general equation applied for given the error in the calculated phase in case of three, four, and five phase stepping algorithms will be:

So,

$$\Delta\Psi_R = \arctan\left[\frac{3\pi/20 - \frac{\pi}{20}\sum_{r=1}^{R}\cos 2(\Psi_R - \alpha_r)}{R - \frac{\pi}{20}\sum_{r=1}^{R}\sin 2(\Psi_R - \alpha_r)}\right] \quad (16)$$

4. Experimental results and discussions

The experimental setup for speckle recording in a $LiNbO_3$ crystal is depicted in Fig. 1. It is utilized as the foundation for developing a productive and easy to use tool for comparison measures. The master (MO) and test (TO) objects are illuminated by almost half of the transmitted beam, also known as the object beam. The pump beam or reference beam, which makes up the remaining fraction of the laser beam, enters the crystal directly. The identical laser source's pump beam is positioned 40 degrees (externally) from the object beam. The result is that the object beam and the bump beam (reference beam) interfere with one another inside the crystal, creating the specklegram.

First, the CCD camera received the wave fields scattered by the test object in its non-displaced state and the wave fields scattered by the master object in both its non-displaced and displaced states, as per the theoretical analysis previously provided. Following the test object's displacement, the two wave fields (non-displaced and displaced states) of the master object and the wave field scattered by the displaced test object make up the interfering beams. The previously stored interferometric speckle pattern was used.

After subtracting the two speckle patterns from one another, the difference, which represented the difference and sum of the displacements of the test and master objects was shown as correlation fringes on the monitor. The sum correlation fringes according to Eq. (9) were also noted, as was previously reported. The measurement's outcome was obtained when the test and master objects were moved axially, as shown in fig. 3 (a, b, c).

This figure illustrates how, for three, four, and five phase stepping algorithms, respectively, the difference correlation fringes and sum correlation fringes coexist when the test and master objects are deformed by 2 µm and 3 µm. A wavelength of 0.6700 µm was employed. Fig. 4 (a ,b ,c) shows the difference correlation fringes coexist with sum correlation fringes when the test and master objects are deformed by 2µm and 3µm respectively, for three, four, and five phase stepping algorithms, respectively. The used wavelength was 0.5780 µm. Fig. 5 (a, b, c) shows the difference correlation fringes coexist with sum correlation fringes when the test and master objects are deformed by 2µm and 3µm respectively, for three- , four-, and five-phase stepping algorithms, respectively. The used wavelength was 0.4360 µm. As we can see from these figures, the visibility of the correlation fringes in case of using five-phase stepping algorithm is better than the correlation fringes obtained using the three- and four-phase stepping algorithms at the same used wavelength.

There is a direct relationship between wavelength and degree of visibility. The degree of visibility decreases as the wavelengths decrease, and vice versa. Depending on equations (11-14), figs. 6a–6c show the unwrapped images using the Itoh algorithm (16), when the test and master objects are deformed by 2µm and 3µm, respectively, for three, four, and five phase stepping algorithms, respectively, in the case of using wavelength 0.6700 μm.

Also, figs 7a-7c and 8a-8b show the unwrapped images using the Itoh algorithm when the test and master objects are deformed by 2µm and 3µm, respectively, for three, four, and five phase stepping algorithms, respectively, in the case of using wavelengths of 0.4360 μm and 0.3600 μm.

These series of figures, which display the data at various wavelengths, demonstrate how the phase unwrapping algorithms work to extract only the difference correlation fringes from the coexisting sum correlation fringes. From there, we can use the phase change to determine the displacement difference between the test object and the master. Depending on equation 15, figs. 9a-9c, 10a-10c, and 11a-11c show the error image due to phase stepper error when the test and master objects are deformed by 2µm and 3µm for three, four, and five phase stepping algorithms, respectively, in the case of using wavelengths of 0.6700 μm, 0.4360 μm, and 0.3600 μm. As we can see from these figures, the visibility of the correlation fringes in the case of using five-phase stepping algorithm is better than the correlation fringes obtained using the three- and four-phase stepping algorithms, even though the wavelength changes. This means that accuracy of the required error measurement is the best at five phase stepping algorithm.

Fig. 12 (a, b, c) show row 310 of the error is due to stepper error, when the test and master objects are deformed by 2µm and 3µm, for three-, four-, and five-phase stepping algorithms, respectively. The used wavelength was 0.6700 μm. Fig. 13 (a, b, c) show row 310 of the error is due to stepper error, when the test and master objects are deformed by 2µm and 3µm, for three-, four-, and five-phase stepping algorithms, respectively. The used wavelength was 0.4360 μm. Fig. 14 (a ,b ,c) show row 310 of the error is due to stepper error, when the test and master objects are deformed by 2µm and 3µm, for three-, four-, and five-phase stepping algorithms, respectively. The used wavelength was 0.3600 μm.

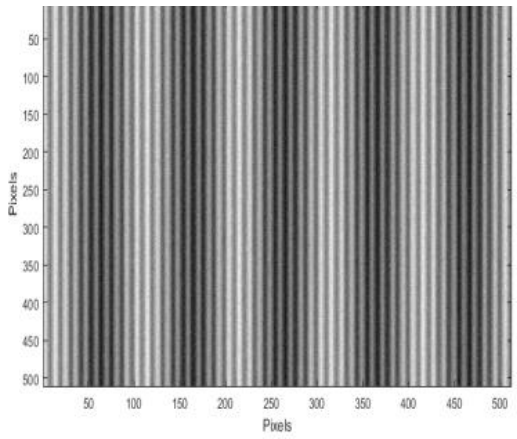

(a)

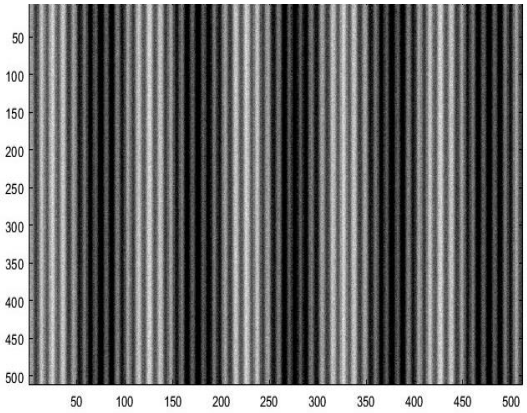

(b)

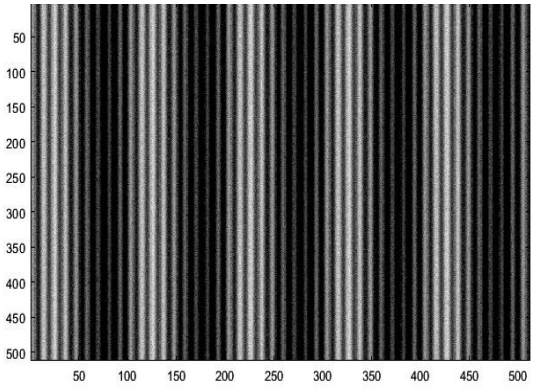

(c)

Fig. 3 (a) Difference correlation fringes coexist with sum correlation fringes for three phase stepping algorithm. **(b)** Difference correlation fringes coexist with sum correlation fringes for four phase stepping algorithm. **(c)** Difference correlation fringes coexist with sum correlation fringes for five phase stepping algorithm. The test and master objects are deformed by 2µm and 3µm respectively. The used wavelength was 0.6700 μm.

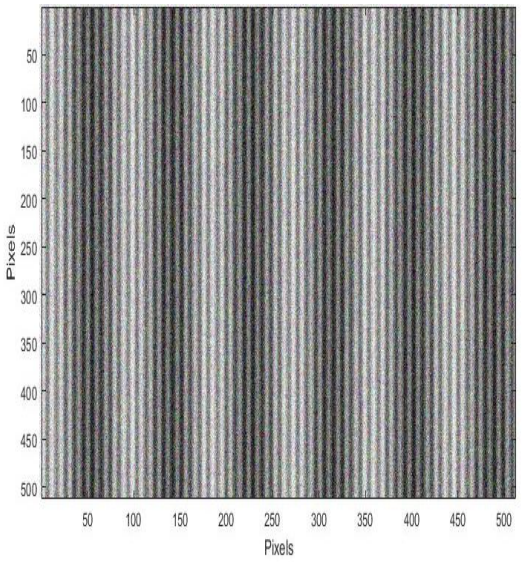

(a)

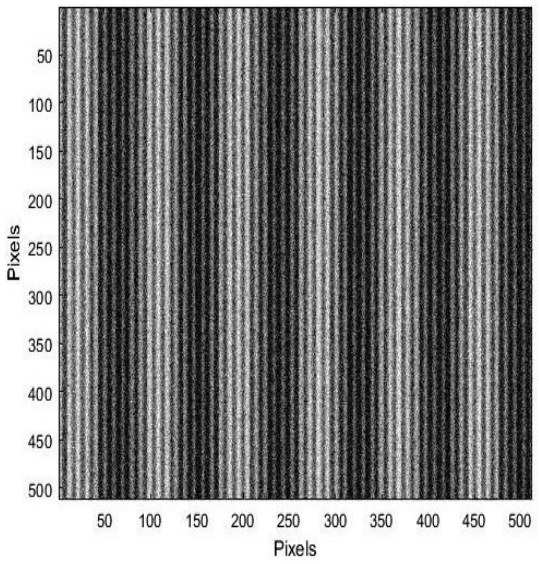

(b)

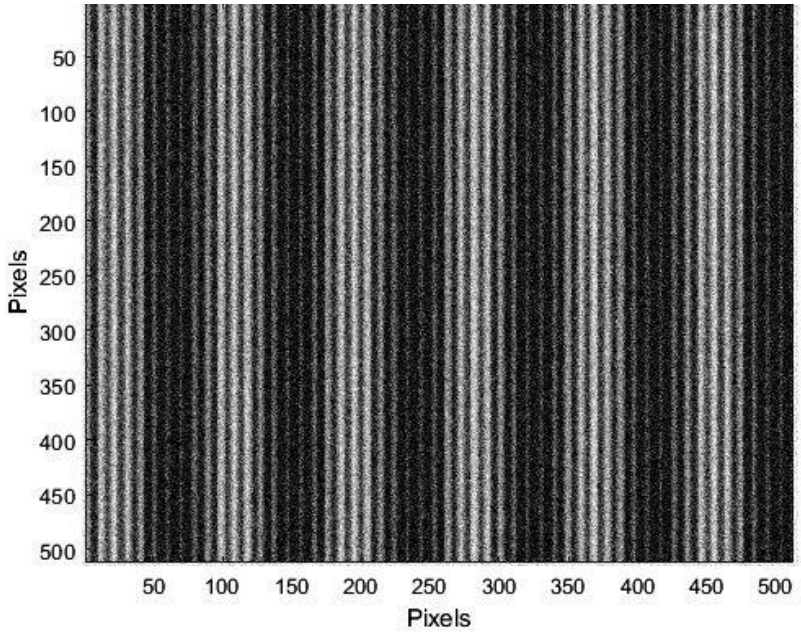

(c)

Fig. 4 (a) Difference correlation fringes coexist with sum correlation fringes for three phase stepping algorithm. **(b)** Difference correlation fringes coexist with sum correlation fringes for four phase stepping algorithm. **(c)** Difference correlation fringes coexist with sum correlation fringes for five phase stepping algorithm. The test and master objects are deformed by 2µm and 3µm respectively. The used wavelength was 0.5780 μm.

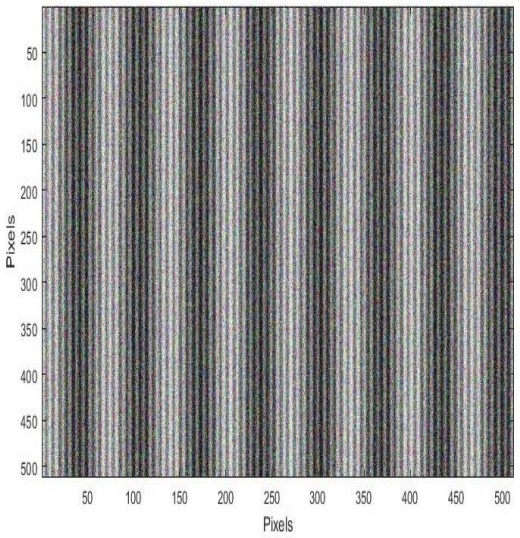

(a)

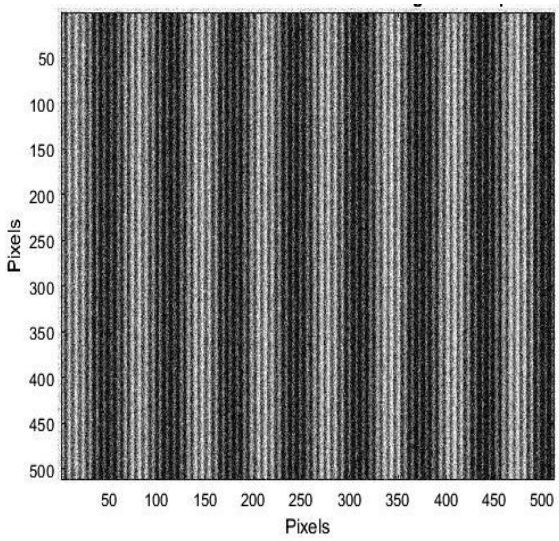

(b)

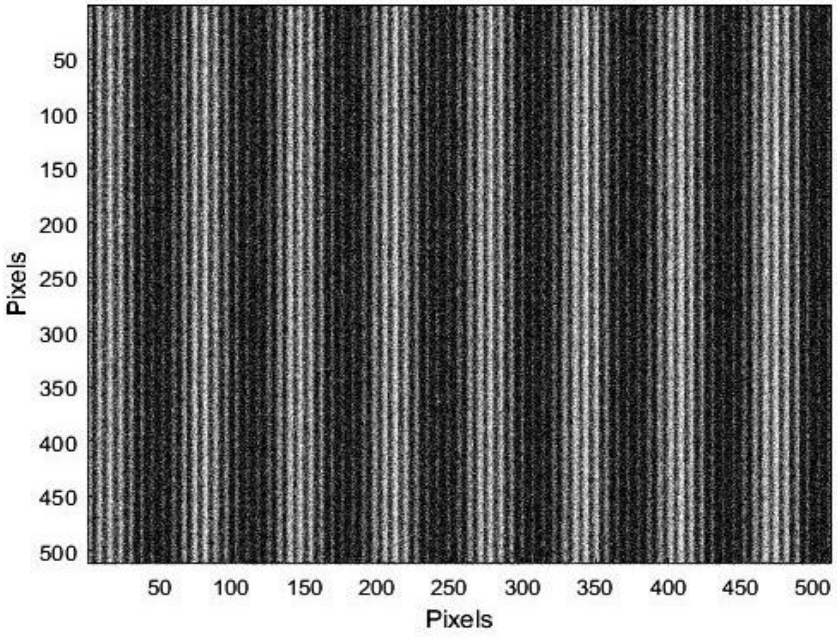

(c)

Fig. 5 (a) Difference correlation fringes coexist with sum correlation fringes for three phase stepping algorithm. **(b)** Difference correlation fringes coexist with sum correlation fringes for four phase stepping algorithm. **(c)** Difference correlation fringes coexist with sum correlation fringes for five phase stepping algorithm. The test and master objects are deformed by 2µm and 3µm respectively. The used wavelength was 0.4360 μm.

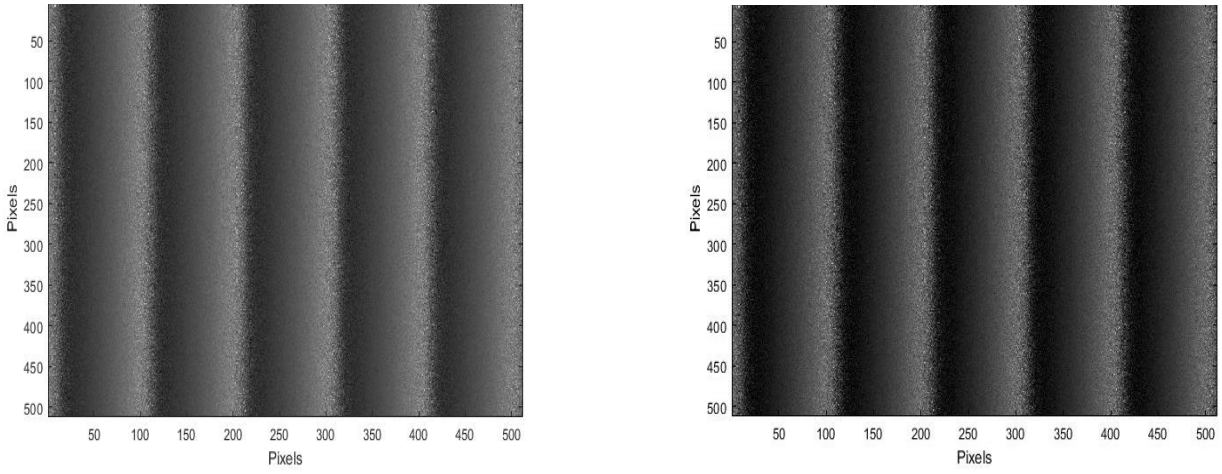

(a) **(b)**

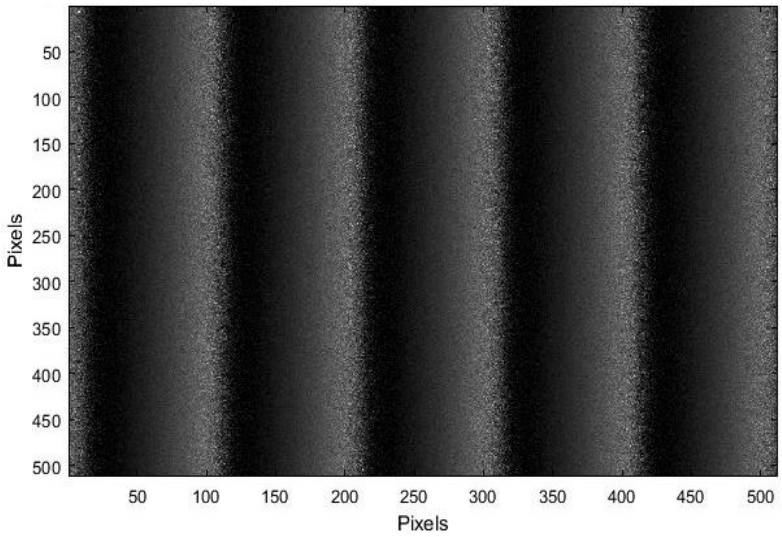

(c)

Fig. 6 (a) Unwrapped images using the Itoh algorithm for three phase stepping algorithm. **(b)** Unwrapped images using the Itoh algorithm for four phase stepping algorithm. **(c)** Unwrapped images using the Itoh algorithm for five phase stepping algorithm. The test and master objects are deformed by 2µm and 3µm, respectively. The used wavelength was $0.6700\mu m$.

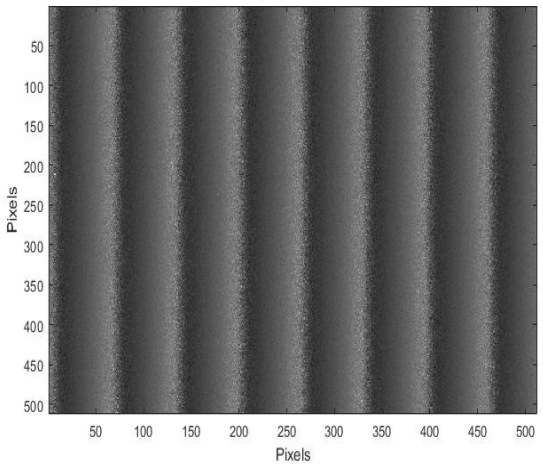

(a)

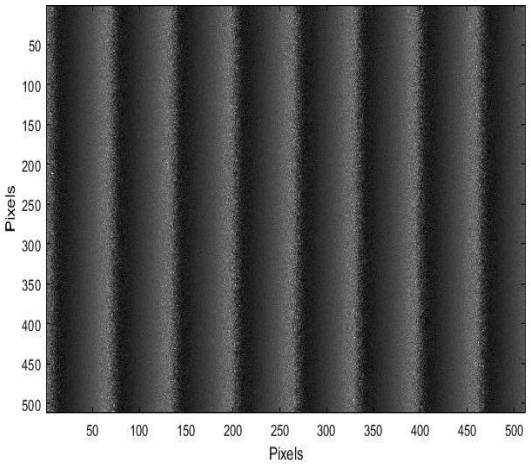

(b)

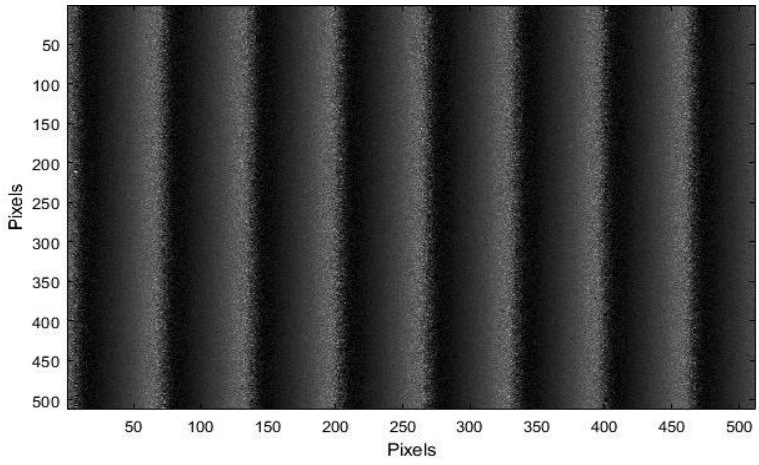

(c)

Fig. 7 (a) Unwrapped images using the Itoh algorithm for three phase stepping algorithm. **(b)** Unwrapped images using the Itoh algorithm for four phase stepping algorithm. **(c)** Unwrapped images using the Itoh algorithm for five phase stepping algorithm. The test and master objects are deformed by 2µm and 3µm, respectively. The used wavelength was $0.4360\mu m$.

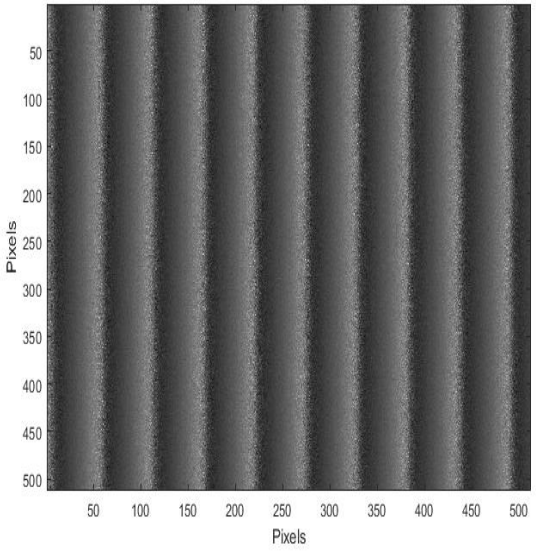

(a)

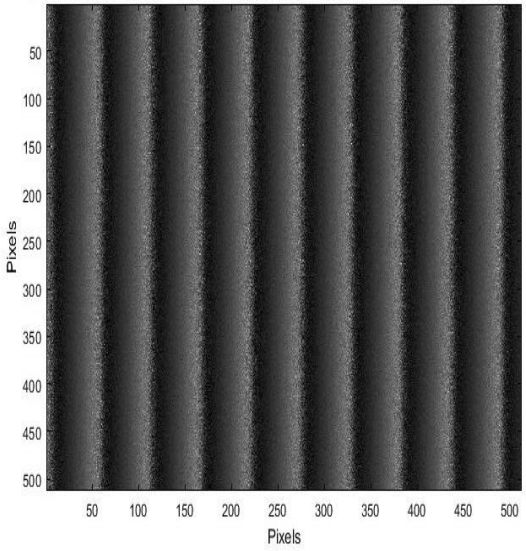

(b)

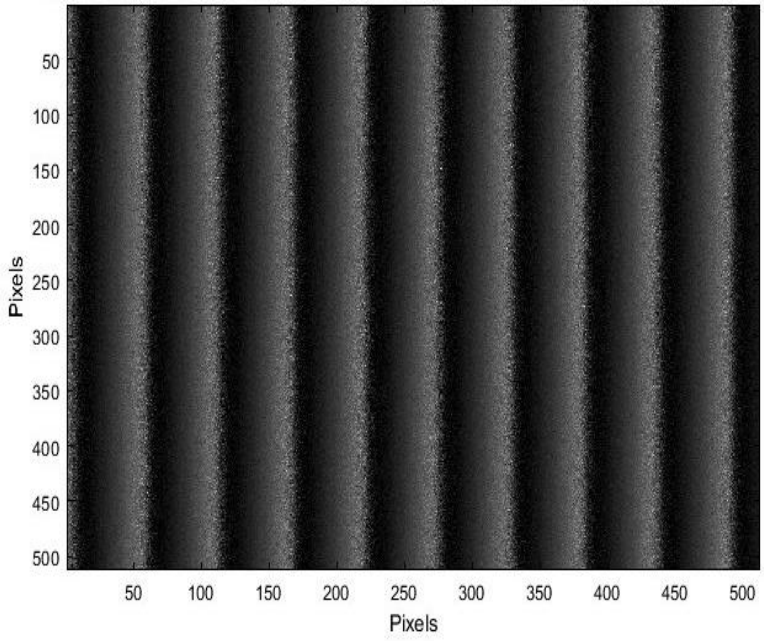

(c)

Fig. 8 (a) Unwrapped images using the Itoh algorithm for three phase stepping algorithm. **(b)** Unwrapped images using the Itoh algorithm for four phase stepping algorithm. **(c)** Unwrapped images using the Itoh algorithm for five phase stepping algorithm. The test and master objects are deformed by 2µm and 3µm, respectively. The used wavelength was $0.3600\mu m$.

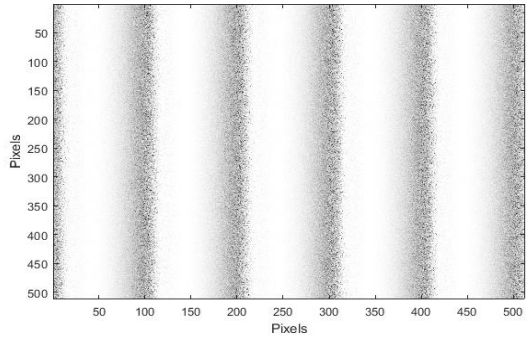

(a)

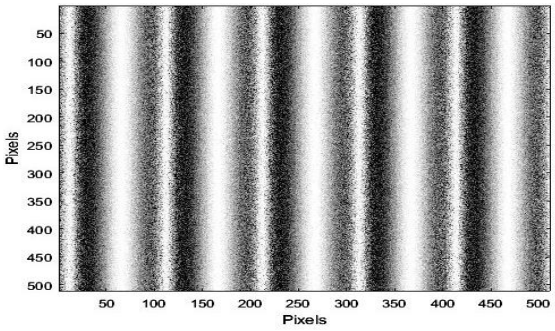

(b)

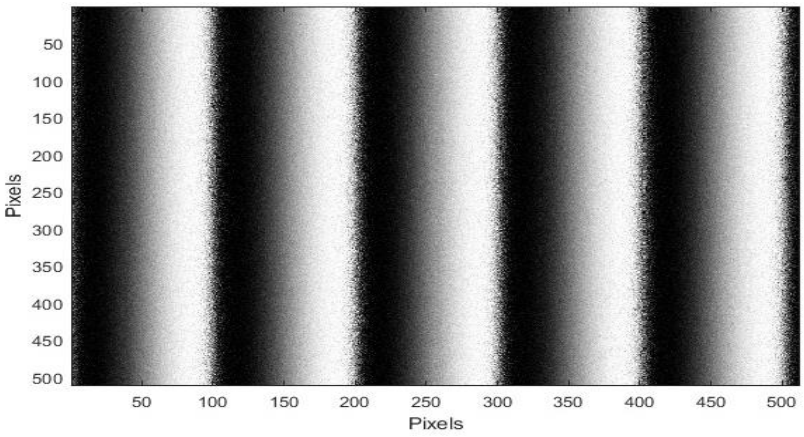

(c)

Fig. 9 (a) Error image due to phase stepper error for three phase stepping algorithm. **(b)** Error image due to phase stepper error for four phase stepping algorithm. **(c)** Error image due to phase stepper error for five phase stepping algorithm. The test and master objects are deformed by 2µm and 3µm respectively. The used wavelength was 0.6700 μm.

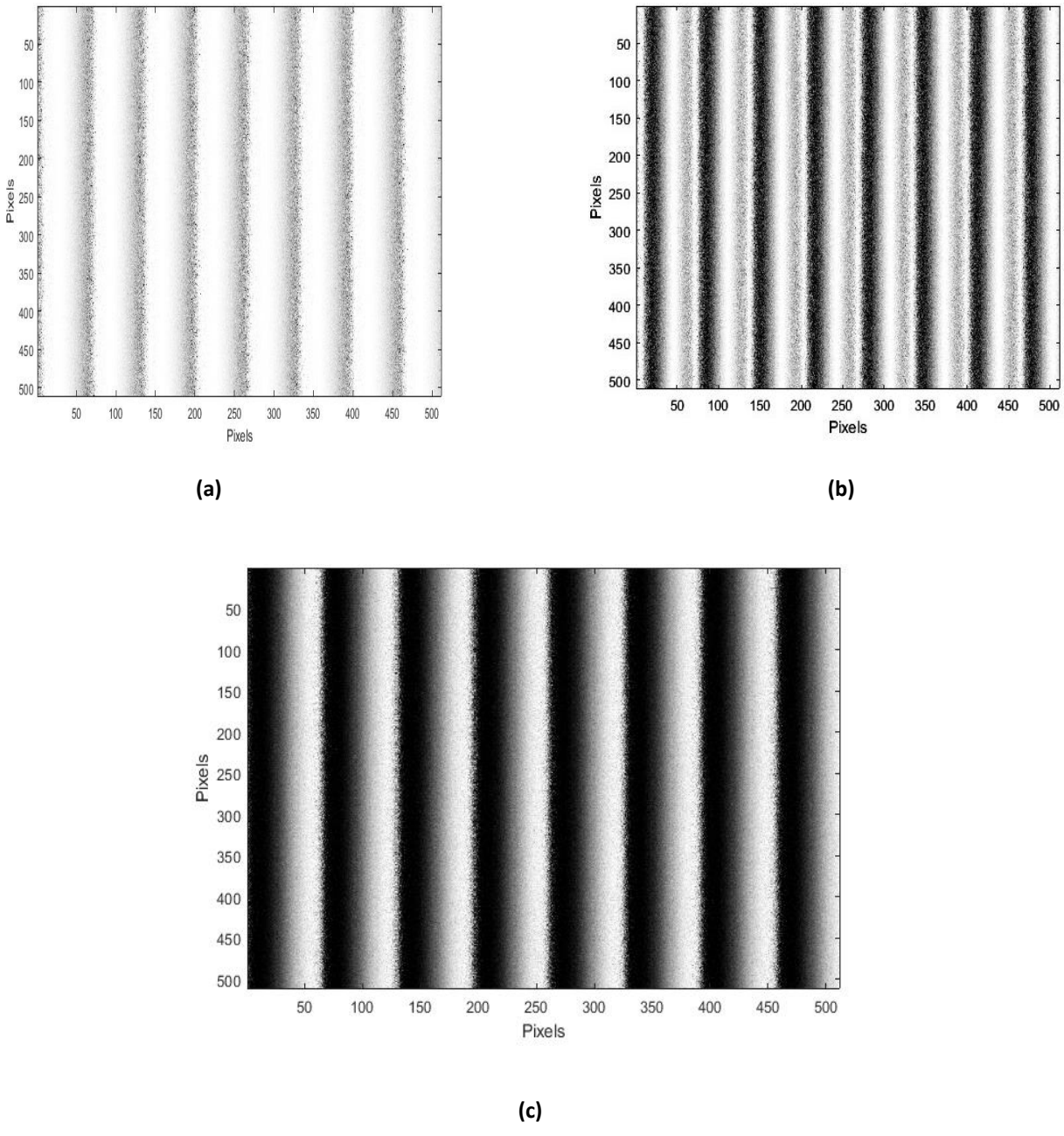

Fig. 10 (a) Error image due to phase stepper error for three phase stepping algorithm. **(b)** Error image due to phase stepper error for four phase stepping algorithm. **(c**) Error image due to phase stepper error for five phase stepping algorithm. The test and master objects are deformed by 2µm and 3µm respectively. The used wavelength was 0. $4360\mu m$.

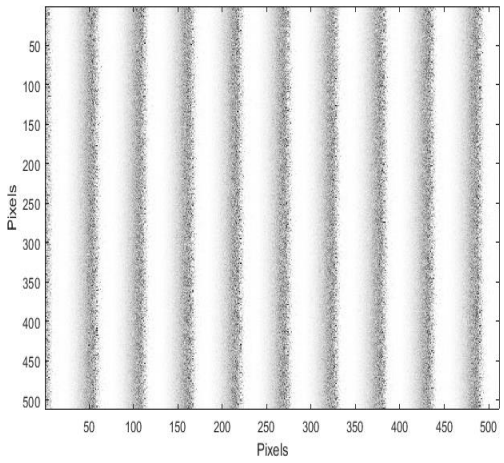

(a)

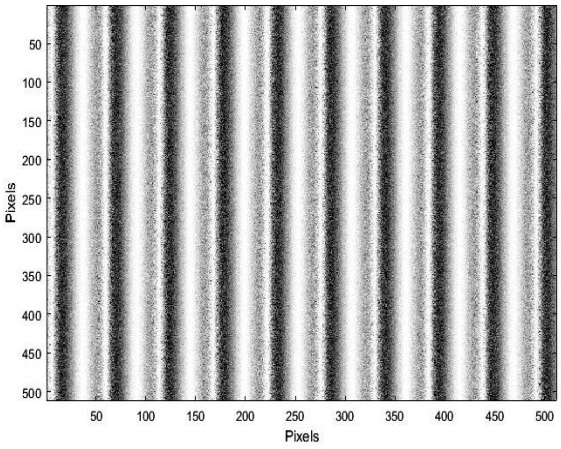

(b)

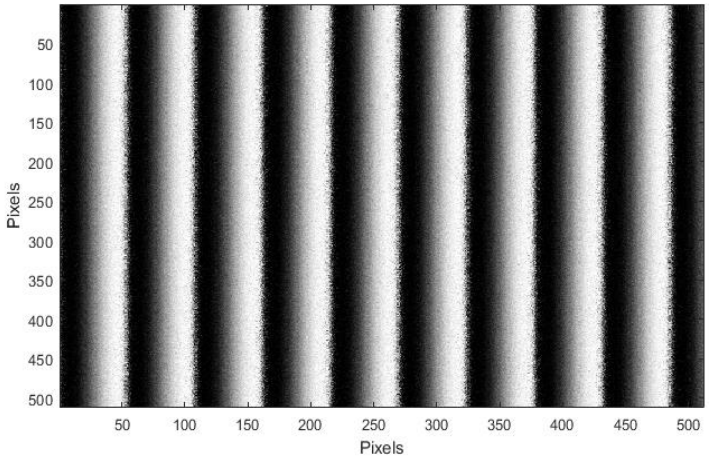

(c)

Fig. 11 (a) Error image due to phase stepper error for three phase stepping algorithm. **(b)** Error image due to phase stepper error for four phase stepping algorithm. **(c)** Error image due to phase stepper error for five phase stepping algorithm. The test and master objects are deformed by 2µm and 3µm respectively. The used wavelength was $0.3600\mu m$.

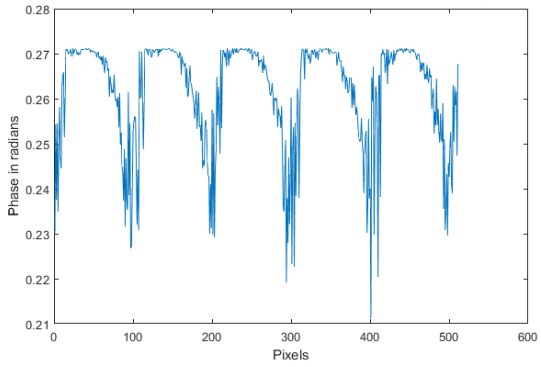

(a)

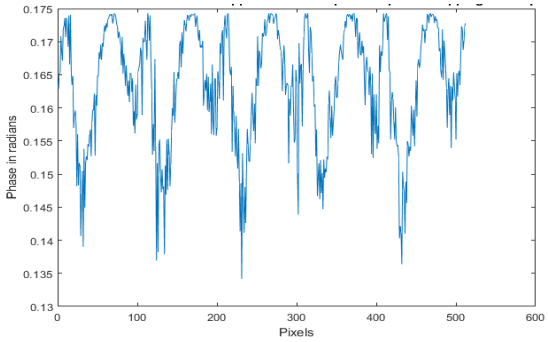

(b)

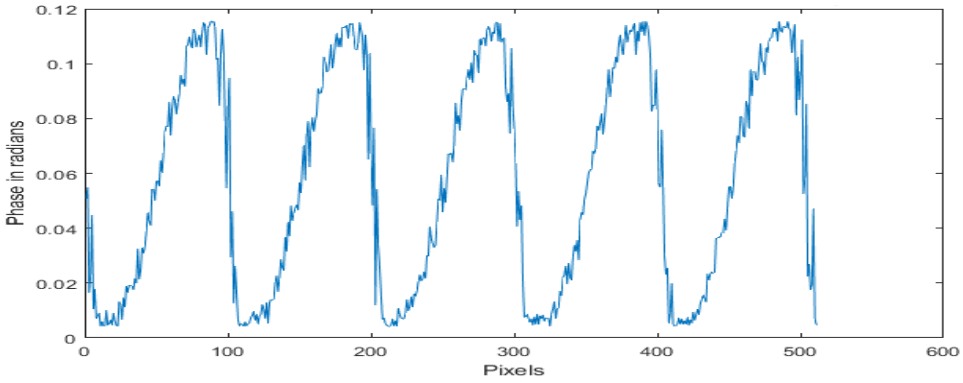

(c)

Fig. 12 (a) Row 310 of the error is due to stepper error for three phase stepping algorithm. **(b)** Row 310 of the error is due to stepper error for four phase stepping algorithm. **(c)** Row 310 of the error is due to stepper error for five phase stepping algorithm. The test and master objects are deformed by 2µm and 3µm respectively. The used wavelength was 0.6700 μm.

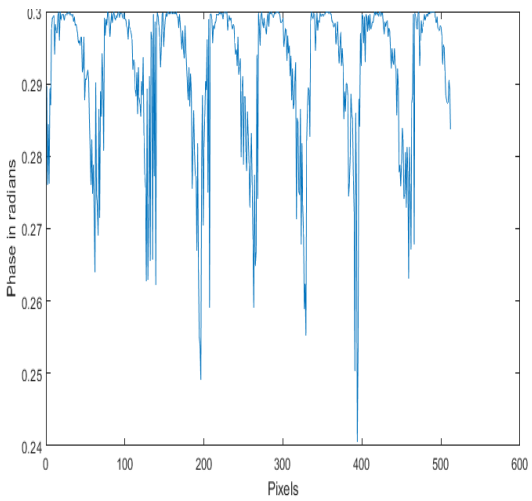

(a)

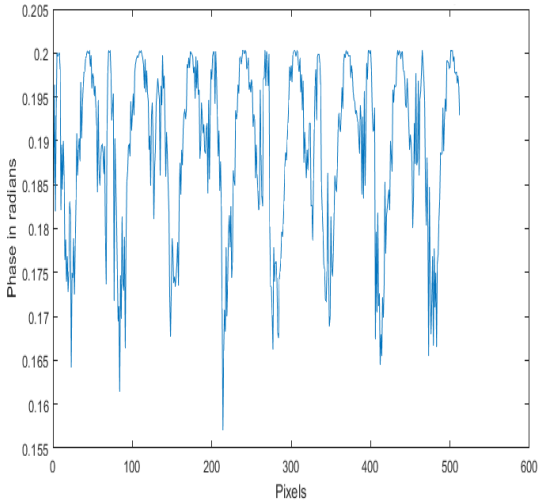

(b)

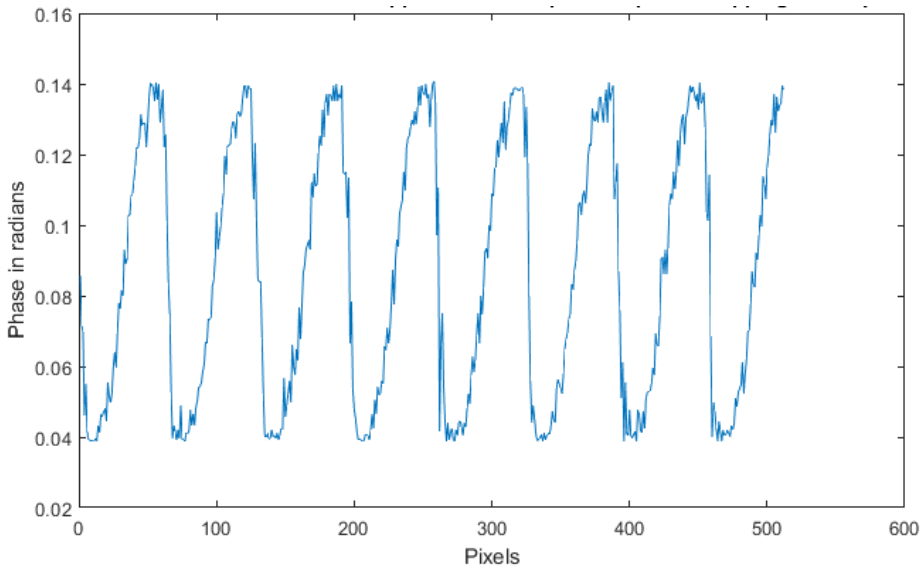

(c)

Fig. 13 (a) Row 310 of the error is due to stepper error for three phase stepping algorithm. **(b)** Row 310 of the error is due to stepper error for four phase stepping algorithm. **(c)** Row 310 of the error is due to stepper error for five phase stepping algorithm. The test and master objects are deformed by 2µm and 3µm respectively. The used wavelength was 0.4360 μm.

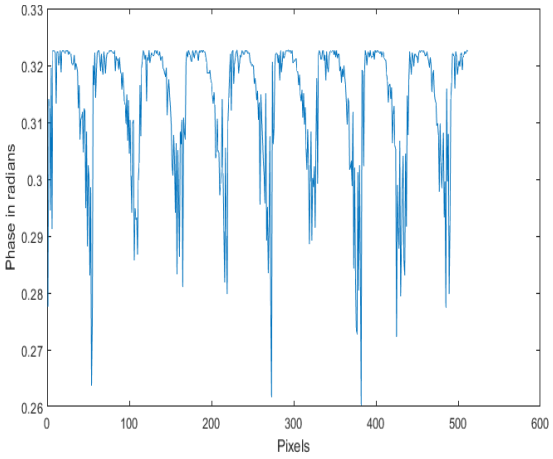

(a)

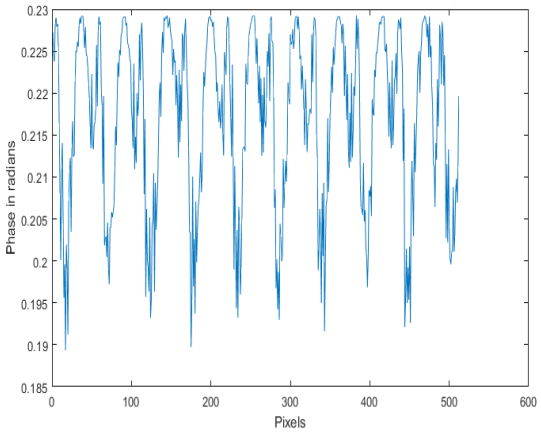

(b)

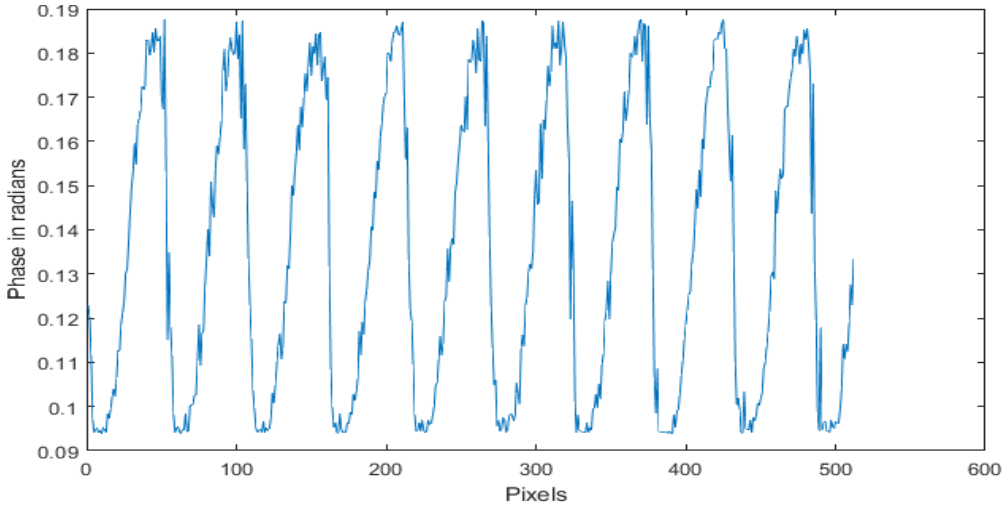

(c)

5. Conclusion

A very precise phase unwrapping method is devised and applied to comparative measurement in phase-shifting digital interferometry to provide the highest level of measurement accuracy. An interferogram that records the differences between the master and test objects that is produced by a single reference beam. Consequently, it is possible to produce difference correlation fringes that coexist with sum correlation fringes. The sum fringes can be removed by applying the phase unwrapping procedures for the fringe analysis. The obtained phase error has the smallest value in the case of the five-phase stepping algorithm compared to the three- and four-phase stepping algorithms at the same wavelength. The visibility of the correlation fringes in the case of using five-phase stepping algorithm is better than the correlation fringes obtained using the three- and four-phase stepping algorithms, even though the wavelength changes.

This means that the accuracy of the required error measurement is the best at the five- phase stepping algorithm. Three, four, and five-phase step algorithms are used to generate a new formula for the addition of the difference and sum phases of deformations and also the error in the computed phase.

6. References

1. **P.K., Rastogi. (1984). Comparative** holographic moiré interferometer in real time, *App. Opt.* **23 (6)**, **924-927** https://doi.org/10.1364/AO.30.000722**.**
2. **Basanta., Bhaduri., M.P., Kothiyal., & N., Krishna Moha. (2008).** A comparative study of phase-shifting algorithms in digital speckle pattern interferometry", Optik, Volume **119,** Issue **3, 22,** pp. **147-152.** https://doi.org/10.1016/j.ijleo.2006.07.014**.**

3. **Chih-Cheng., Kao., Gym-Bin., Yeh., Shu-Sheng., Lee., Chih-Kung., Lee., Ching-Sang., Yang., and Kuang-Chong., Wu. (2002).** Phase-shifting algorithms for electronic speckle pattern interferometry, Appl. Opt. Vol. **41,** No. **1/1** January **46-54.** https://opg.optica.org/ao/abstract.cfm?URI=ao-41-1-46
4. **Amalia., Martínez., Juan Antonio., Rayas., & Raul., R. Cordero. (2009).** Measurement of in plane strain with shearography and electronic speckle pattern interferometry, Revista Mexicana de Físíca **57 (6): 217–226** DOI:10.1109/ISOT.2014.52**.**
5. **Nasser., A.Moustafa., Janos., Kornis., & Zoltan., Füzessy. (1999).** Comparative measurement by phase-shifting digital speckle interferometry using holographically generated reference wave, *Opt. Eng*. **23(7), 1241-1245** Corpus ID:122186582.
6. **Bing., Zhao., and Yves., Surrel. (1995).** Phase shifting: six-sample self-calibrating algorithm insensitive to the second harmonic in the fringe signal, Optical Engineering, **34(9):2821-2822** DOI:10.1117/12.211676.
7. **Yves., Surrel. (1996).** Design of algorithms for phase measurements by the use of phase stepping", *Applied Optics*, Vol**. 35,** Issue **1, pp. 51-60** https://doi.org/10.1364/AO.35.000051.
8. **K., Itoh. (1982).** Analysis of the phase unwrapping algorithm, *Appl Opt.* Jul **15;21(14):2470**. https://doi.org/10.1364/AO.21.002470.
9. **Dennis., C., Ghiglia., Mark., D., Pritt. (1998).** Two-Dimensional Phase Unwrapping: Theory, Algorithms, and Software", May ISBN: 978-0-471-24935-1.
10. **Nasser., A.Moustafa., J., Kornis., and Z., Füzessy. (1999).** Comparative measurement in speckle interferometry using holographically generated reference wave by single reference beam technique, Opt. Commun. **172 (1-6) 9-16.** https://doi.org/10.1016/S0030-4018(99)00415-0.
11. **Nasser., A. Moustafa. (2020).** Measurement Uncertainty of In-Plane Displacement Field Distribution Using Speckle Photography With LiNbO3 Crystal", **Opt. Eng. 59(2), 024108** http://doi:10.1117/1.OE.59.2.024108.
12. **Nicolaus., R. A. (1990).** Evaluation of Fizeau interferences a comparison of phase-stepping algorithms, *Proc. SPIE* **1319, 237-238.** DOI:10.1117/12.22296
13. **B. T., Matthiar., and J. P., Remeika. (1949).** Ferroelectricity in the Ilmenite Structure, Phys. Rev. **76,** pp. **1886-1887** https://doi.org/10.1103/PhysRev.76.1886.2
14. **B.K., Vainshtein. (1981).** Modern Crystallography 1, Springer Ser. Solid-State Sci., Vol. **15** (Springer, Berlin, Heidelberg, New York ISBN-10. 0387100520.
15. **Sujoy., Sinha Roy., Chester., Rebeiro., & Debdeep., Mukhopadhyay. (2011).** Theoretical modeling of the Itoh-Tsujii Inversion algorithm for enhanced performance on k-LUT based FPGAs, Design, Automation and Test in Europe Conference and Exhibition, **14-18** March DOI:10.1109/DATE.2011.5763197
16. **T., Itoh., and S., Tsujii. (1988).** A Fast Algorithm for Computing Multiplicative Inverses in GF (2*m*) Using Normal Bases. *Information and Computation*, **78:171–177,** https://doi.org/10.1016/0890-5401(88)90024-7
17. **Schwider., J., Burow., R., Elssner., K. E., Grazanna., R., Spolacyk., R., and Merkel., K. (1983).** Digital wavefront measuring interferometry: some systematic error sources, Appl. Opt. **22, 421-3432.**https://doi.org/10.1364/AO.22.003421**.**
18. **Van Wingerden., T., Frankena., H. J., & Smorenburg., C. (1991).** Linear approximation for measurement errors in phase shifting interferometry, Appl. Opt. **30, 2718-2729.** http://doi.org/10.1364/AO.30.002718
19. **Gisela., Domínguez-Guzmán., J., Castillo-Mixcóatl., Georgina., Beltran Perez., S., Muñoz-Aguirre. (2009).** Itoh algorithm to unwrap 2D phase, September, Proceedings of SPIE - The International Society for Optical Engineering. DOI:10.1117/12.851057.